NUMERICAL SIMULATION OF BUBBLE-TRAIN FLOW IN A SMALL CHANNEL OF SQUARE CROSS-SECTION

B. Ghidersa, M. Wörner, D.G. Cacuci

Forschungszentrum Karlsruhe GmbH
Institut für Reaktorsicherheit
Postfach 36 40, 76021 Karlsruhe, GERMANY
Phone: +49 7247 82-3764, Fax: +49 7247 82-3718,
E-mail: ghidersa@irs.fzk.de

ABSTRACT

Bubble-train flows in small channels are widely used in industrial applications due to their good mixing properties and heat transfer enhancement. In this paper, the three-dimensional flow structure of a bubble-train flow in a square capillary is analyzed using direct numerical simulation. For a fixed value of the void fraction ($\varepsilon = 33\%$) the influence of the interface surface tension is studied by considering two different values of the Capillary number. Comparison of the computed global parameters with experimental data reported in the literature for these values of the Capillary number shows good agreement.

1. INTRODUCTION

Flow channels with hydraulic diameters (D_h) of 1mm or below are applied e.g. in compact heat exchangers, microelectronic cooling systems, chemical processing, or small-sized refrigeration systems. In many of these applications frequently gas-liquid two-phase flow occurs. Because the importance of surface tension increases with decreasing channel size, the hydrodynamics of gas-liquid two-phase flow in small channels in principal differ from that in larger channels. For design, optimization and safe operation of devices built from micro-channels the understanding of the basic hydrodynamic phenomena in a single channel is mandatory. This motivates an increasing number of experimental and theoretical studies devoted to this topic. Recently, Triplett et al. ([1],[2]) studied the two-phase flow patterns, void fraction and the pressure drop of air-water two-phase flows in a horizontal circular or triangular channel with diameters of order of 1 mm. Depending on the gas and liquid flow rates, bubbly, slug, churn and annular flow regimes have been identified. For both circular and triangular channels the flow pattern transition is different than the one predicted using large channels correlations.

The present numerical study investigates the slug flow in straight capillaries of square cross-section. This type of flow, also referred as bubble-train flow [3], consists of trains of long bubbles separated by liquid slugs. The bubbles occupy most of the channel cross-section while the liquid slugs are free of smaller bubbles [1]. Breakage and coalescence of bubbles is largely absent. Due to the dominance of the surface tension effects the walls are always wetted and a thin liquid layer separates the gas from the channel walls. Bubble-train flow is very effective to increase heat and mass transfer rates compared to single-phase and therefore is widely used in gas-liquid processing. Thulasidas et al. [3] examined the bubble size and shape, bubble velocity, and volume fraction of gas inside capillaries of circular and square cross-section for slug flow regime. These parameters are of significant interest in predicting the mass transfer rates between the fluid and the wall. Thulasidas et al. [4] uses a particle imaging velocimetry (PIV) to determine the velocity distribution inside the liquid slug. Video images recorded in a reference frame moving with the bubble indicate

the presence of recirculating patterns with a high degree of mixing. Depending on the capillary number of the flow, counter rotating vortices or a complete bypass flow inside the liquid slug were observed.

While these experimental approaches offer the advantage of dealing directly with the physical problem they have limited access to the local characteristics of the flow in small channels, where only non-intrusive methods can be used. Our goal here is to study the local characteristics of the flow by means of direct numerical simulation (DNS). For this we use an extended and improved version of our in-house computer code TURBIT-VOF [5], which was originally developed for investigation of bubbly flow in large channels. To account for the phase-interface evolution the volume fraction of the continuous phase is tracked using a Volume of Fluid method. A short description of the equations and the computer code TURBIT-VOF will be given in section 2 while the numerical set-up will be described in section 3. The structure of the flow inside the bubble and in the liquid phase will be then analyzed for bubble-train flows at two different values of Capillary number. To validate our method the numerical results will be compared with experimental data from the literature. In section 5 we present the conclusions.

2. MATHEMATICAL AND NUMERICAL BACKGROUND

The direct numerical simulations are performed with an extended and improved version of our in-house computer code TURBIT-VOF [1]. The code is based on a single set of equations for the entire domain, which expresses the conservation of mass, momentum and enthalpy for a continuous Newtonian fluid [6]. Starting from the local instant equations, a set of volume-averaged equations for each phase are written. These equations and the local interface jump conditions are used to write a single set of equations for the mean values of the variables. These mean values are defined in terms of volume averaging.

If V is a control volume, which, in our case, is taken to be a computational cell, for incompressible fluids, the dimensionless continuity equation becomes

$$\nabla \cdot \vec{v}_m = 0 \tag{1}$$

while the momentum equation, in dimensionless form, is

$$\frac{\partial \rho_m \vec{v}_m}{\partial t} + \nabla \cdot \rho_m \vec{v}_m \vec{v}_m = -\nabla P + \frac{1}{Re_{ref}} \nabla \cdot \underline{\underline{\tau}}_m - (1-f)\frac{E\ddot{o}_{ref}}{We_{ref}}\frac{\vec{g}^*}{g^*} + \frac{1}{We_{ref}}\kappa \vec{n} a_{int} \tag{2}$$

where, f is the liquid volume fraction within the averaging volume V, and ρ_m is the dimensionless mean density,

$$\rho_m = \frac{f\rho_l^* + (1-f)\rho_g^*}{\rho_l^*}. \tag{3}$$

In (2) we use the reduced pressure P, which is the difference between the pressure p in that point and the liquid hydrostatic pressure in the same point $\left(\dfrac{\vec{x}^* \cdot \vec{g}^*}{L_{ref}^* (v_{ref}^*)^2} \right)$. Due to this, the influence of the gravity in the momentum equation is accounted by a buoyancy term. The last term in (2) expresses the contribution of the surface tension forces in the momentum balance for the volume V. There, κ is the interface curvature, $\vec{n}$ is the unit normal vector to the interface, pointing from the gas into the liquid, and a_{int} is the interfacial area concentration within the volume V. In the previous equations the superscript (*) denotes dimensional quantities, while the subscript m denotes the mean value of the corresponding quantity. The dimensionless momentum equation has been obtained using the

liquid inertia $\rho_l^* \left(v_{ref}^* \right)^2$ as reference scaling quantity. Thus, the definitions of the reference Reynolds number $\left(Re_{ref} \right)$, reference Weber number $\left(We_{ref} \right)$ and reference Eötvös number $\left(E\ddot{o}_{ref} \right)$ appearing in (2) are:

$$Re_{ref} = \frac{\rho_l^* L_{ref}^* v_{ref}^*}{\mu_l^*} \; ; \tag{4}$$

$$We_{ref} = \frac{\rho_l^* L_{ref}^* \left(v_{ref}^* \right)^2}{\sigma^*} \; ; \tag{5}$$

$$E\ddot{o}_{ref} = \frac{\left(\rho_l^* - \rho_g^* \right) g \left(L_{ref}^* \right)^2}{\sigma^*} . \tag{6}$$

To account for the phase-interface evolution the volume fraction of the continuous phase is tracked using a Volume of Fluid procedure. Thus, the liquid volumetric fraction is advected using the transport equation

$$\frac{\partial f}{\partial t} + \nabla \cdot \left(\vec{v}_m f \right) = 0 \tag{7}$$

while the interface inside each volume V is reconstructed using the PLIC (<u>P</u>icewise <u>L</u>inear <u>I</u>nterface <u>C</u>alculation) method EPIRA (for details, see [5]).

To numerically integrate the momentum equation (2) while enforcing the continuity condition (1) a projection method is used: first, an intermediate velocity field is computed using the equation (2) in which the pressure gradient is neglected. The time integration is done using a third order Runge-Kutta scheme. A second order central difference scheme is used to approximate the convective and diffusive terms. For the discretization of the surface tension term we refer to [5]. This velocity field is not divergence-free. To obtain a velocity that satisfies the continuity condition (1) a projection step is required, that is, compute the pressure gradient that we have neglected in the previous step and construct the projection operator. This operator is then applied to the intermediate velocity field. Special care is taken when the gradient of the (physically discontinuous) pressure at the phase-interface is computed.

The form of the equations (1), (2) and (7) as given above already implies that within volume V both phases have the same volume-averaged velocity and that there is no phase transfer across the interface, i.e. the velocity is continuous. The first assumption corresponds to a locally homogenous model [6].

3. NUMERICAL SETUP

In small channels, the channel length is typically much larger than its hydraulic diameter, therefore, one can identify a region where there is no influence of the entrance effects and the bubbles have identical shape, they move with the same velocity and are uniformly distributed along the channel. Thus, one can define a fluid cell consisting of a bubble and the slug in the rear of the bubble that fully characterizes the bubble-train flow in the steady region. Experimentally, the measurements are done by following the fluid cell in its movement along the channel by a moving camera. Numerically, we define the computational domain so that it has the same dimensions as the fluid cell. This domain is fixed while the bubbles move through it (see Figure 1). The presence and influence of the neighboring cell is simulated using periodic boundary conditions in streamwise direction.
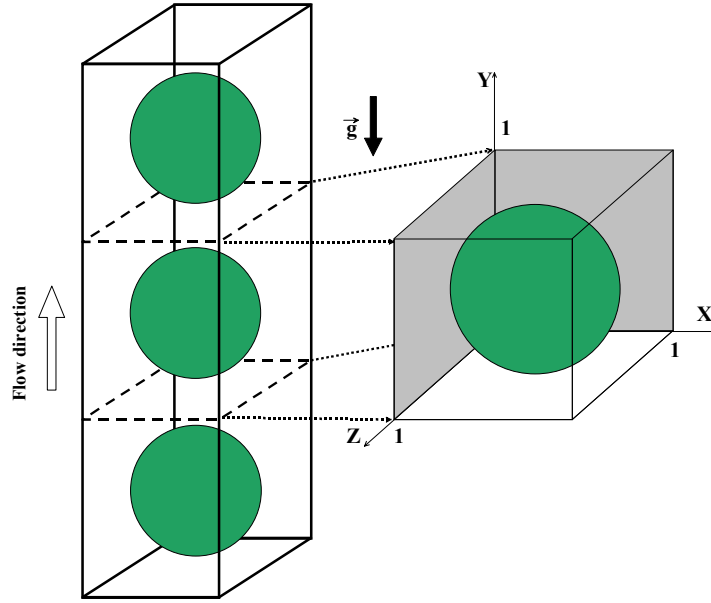
Figure 1. Computational domain and initial condition

For the present study we consider the case where the length L_y^* of the fluid cell is the same as the width of the channel $L_x^* = L_z^* = L_{ref}^*$. In Figure 1 the coordinate system and a sketch of the computational domain is presented. The computational domain in terms of L_{ref}^* is $1\times1\times1$ and is discretized by 64^3 uniform mesh cells. The flow is in y-direction while in the other two directions walls bound the domain where no-slip boundary conditions are used.

The simulation is started from an initially spherical bubble with diameter $d^* = 0.858\ L_{ref}^*$; this corresponds to an overall void fraction of $\varepsilon = 33\%$. To establish a specific overall flow rate a constant pressure drop is imposed in y-direction.
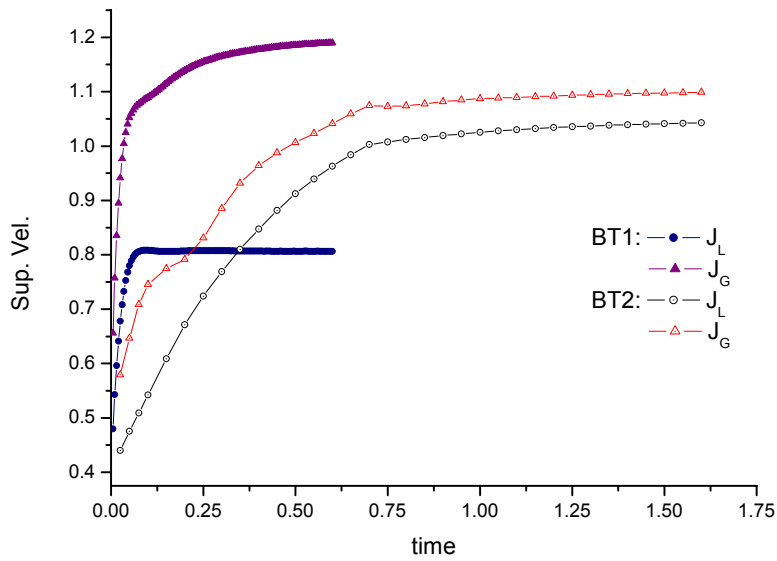

Figure 2 Time evolution of the dimensionless liquid and gas superficial velocities.

4. RESULTS AND DISCUSSIONS

In this section we present the results for two different cases (Table I). Initially the flow is accelerated but, after a transient, the simulation results in a fully developed regime with constant gas and liquid flow rates (Figure 2). In the first case (BT1) we simulate a flow for which the kinematic viscosity of the liquid is three times larger than for the gas. After $t = 0.6$, the bubble shape and velocity are steady. Because of the high value of the liquid viscosity the liquid layer near the wall is thick and the bubble is axisymmetric.

Table I Simulation parameters. The *Re* and *Eö* numbers are computed using the bubble diameter and bubble velocity as reference length, and velocity, respectively.

|	ε	ρ_g/ρ_l	μ_g/μ_l	*Re*	*Eö*	$-\Delta p/L$	J_L	J_G
BT1	33 %	1/81	1/260	1.35	1.065	27	0.806	1.189
BT2	33 %	1/78	1/25	75.88	1.347	0.2	1.04	1.10

In the second case (BT2) the liquid is taken to be less viscous than in the first case, therefore it takes more time for to have a steady bubble shape and bubble velocity ($t = 1.0$). The bubble diameter becomes larger than in the (BT1) case and almost fills the channel width. Since the liquid film in the axial planes becomes very thin the liquid is pushed to the corners of the channel and it is strongly accelerated. This results in a stronger mixing both in the liquid slug and inside the bubble. The flow inside the bubble for the two cases is compared in Figure 3. For that, we consider the referential linked to the bubble center of mass and insert massless particles into the flow at different position inside the bubble. Since the flow is steady and the bubbles move with constant speed there is no need to take in to account acceleration effects. For (BT1) the gas inside the bubble forms a single annular vortex while in (BT2) a second vortex appears at the rear side of the bubble. The presence of the second vortex can be explained by a more intense recirculation in the liquid slug.

The strong mixing inside the bubble is of great interest in chemical processing where the bubbles are used as micro-reactors in which the precipitation reagents are thoroughly mixed avoiding the heterogeneous reaction conditions in classical large batch reactors. For the heat exchangers, the structure of the flow inside the liquid is more important. In Figure 4 the flow in the liquid layer between the bubble and the walls and in the liquid slug is presented. Again, a referential linked to the bubble is used. The massless particles are inserted in front of the bubble (y=1). At the corner of the channel the particles have a rectilinear trajectory and their velocity is almost constant along the channel. Close to the bubble, particles are accelerated as they approach the cross-section where the bubble has the larger diameter, and then decelerate, some of the particles being captured in the vortex behind the bubble. For the BT2 case, the presence of the second vortex inside the bubble generates also two vortices in the liquid slug: one close to the rear side of the bubble that is coupled with the vortex at the bottom of the bubble, and a second one coupled with the vortex at the top of the next bubble.

In order to assess our numerical code we compare the results with the experimental data obtained by Thulasidas *et al.* [3] (Figure 5). They measured the bubble diameter and the bubble velocity for a bubble-train flow in a square channel with a hydraulic diameter of 2mm. From the measured values they compute the dimensionless bubble diameter D_B/D_h, dimensionless bubble velocity $U_B/(J_L + J_G)$, and the relative bubble velocity $W = (U_B - v_{ls})/U_B$, where v_{ls} is the liquid slug velocity. They plot their results as a function of the Capillary number of the flow $Ca = \mu_l U_B/\sigma$. The values of these parameters obtained from the numerical simulations are given in Table II.

Table II Computed Capillary number, dimensionless bubble diameter, bubble velocity and relative bubble velocity.

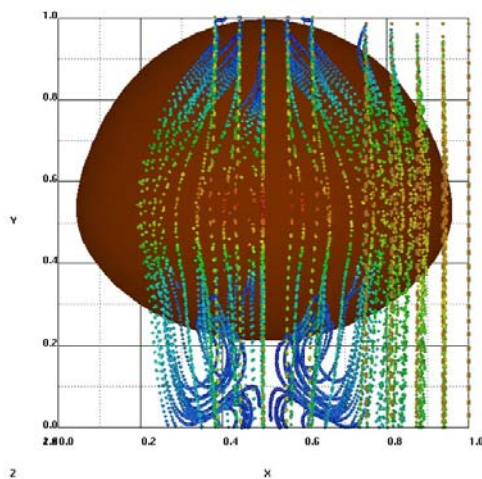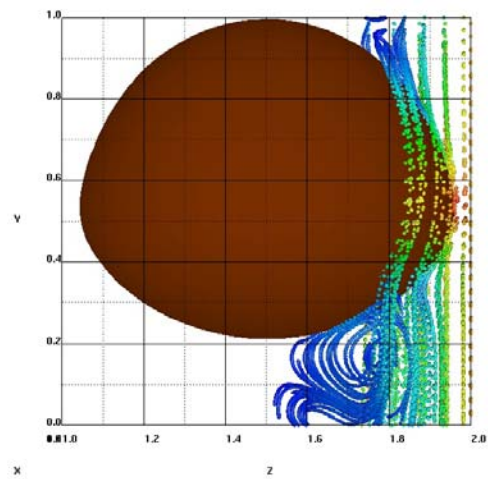|	Ca	D_B/D_h	$U_B/(J_L+J_G)$	W
BT1	0.205	0.798	1.80	0.445
BT2	0.043	0.919	1.55	0.355
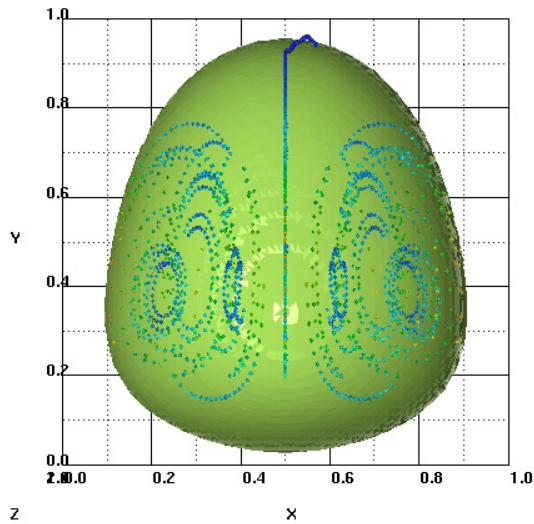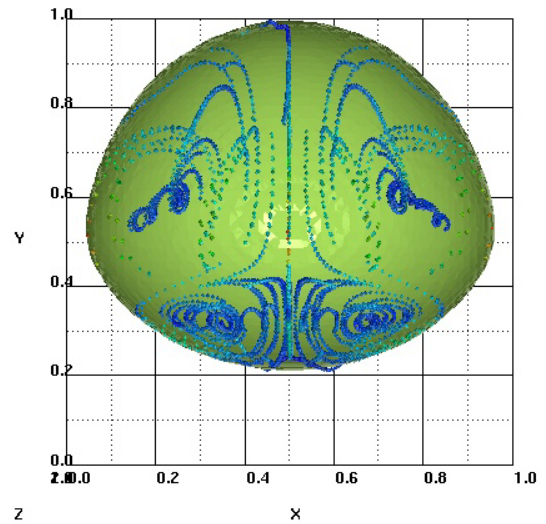
(BT1) $t = 0.6$ (BT2) $t = 1.4$

Figure 3 Visualization of the flow structure inside the bubble. Massless particles were inserted inside the bubble and advected by the velocity field, in a referential linked to the bubble center of mass.
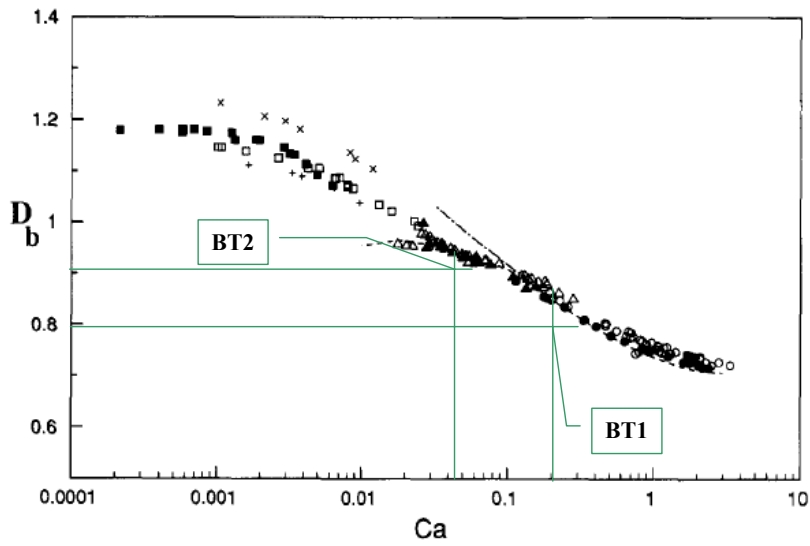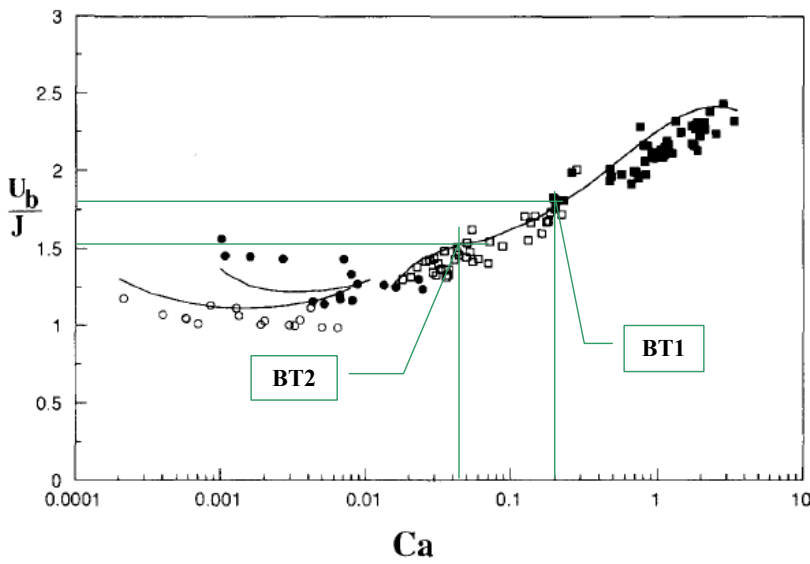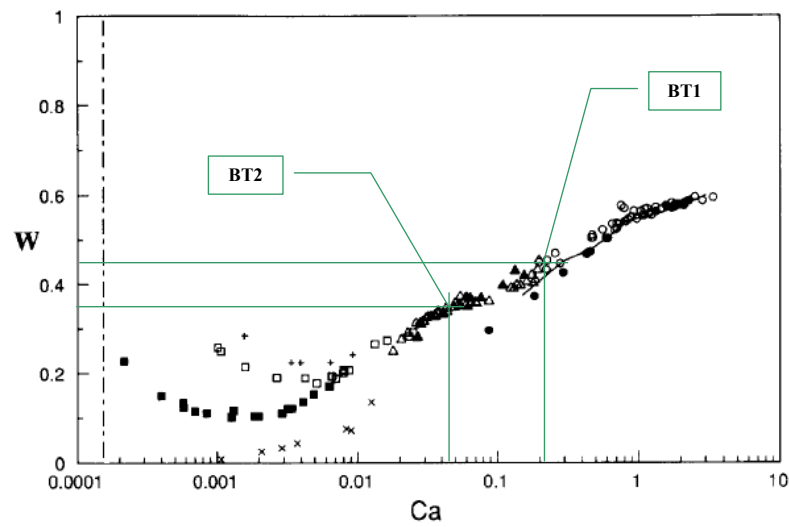

(a)

(b)

Figure 4 Visualization of the flow structure in the liquid for the BT2 case: front view (a); lateral view (b). A referential linked to the bubble center of mass is used. The massless particles are inserted in the top of the computational domain and they move along the current lines of the flow.

Figure 5 Comparison of the computed values (Table II) with experimental data from Thulasidas *et al.* [3]: (a) dimensionless bubble diameter; (b) dimensionless bubble velocity ($J = J_L + J_G$); (c) relative bubble velocity ($W = (U_B - v_{ls})/U_B$). Reproduced from [3].

For the dimensionless bubble diameter (Figure 5.a) the computed values are slightly smaller than the measured values. This difference can be explained by the fact that in experiments the bubbles have the length several times the channel width and the diameter is measured in the cylindrical part while in our computations the bubbles are much shorter and can not develop in a Taylor bubble. For the bubble velocity and relative bubble velocity we have a better agreement, the computed values being in the range of the measured data (Figure 5.b, c).

5. CONCLUSIONS

In the present paper we use direct numerical simulation to investigate the local characteristics of a bubble-train flow in a channel with square cross-section. Using the computed three dimensional flow field we were able to visualize the structure of the flow inside the bubble and in the liquid. For low Ca flow a second vortex appears both in the liquid slug and inside the bubble increasing the mixing properties of the flow. Also, flow parameters like bubble shape and diameter and bubble velocity, which are of significant interest in predicting the mass transfer rates between the fluid and the wall, have been computed. Comparison of the computed global parameters with experimental data reported in the literature for the same values of the Capillary numbers shows good agreement.

NOMENCLATURE

a_{int}	interfacial area concentration		Greek symbols	
Ca	Capillary number			
D	diameter		ρ	density
$E\ddot{o}$	Eötvös number		κ	interface curvature
f	liquid volume fraction		τ	stress tensor
g	gravitational acceleration		σ	surface tension coefficient
J	superficial velocity		ε	total void fraction
L	reference length		μ	viscosity
P	pressure			
Re	Reynolds number		Subscripts	
U	bubble velocity			
V	control volume		G,g	gas phase
$\vec{v}$	velocity		L,l	liquid phase
v_{ls}	liquid slug velocity		m	volume averaged value
W	relative bubble velocity		ref	reference quantity
We	Weber number			

REFERENCES

[1] Triplett, K.A., Ghiaasiaan, S.M., Abdel-Khalik, S.I., Sadowski, D.L., Gas-liquid two-phase flow in microchannels; Part I: two-phase flow patterns. Int. J. Multiphase Flow, Vol. 25, pp. 377, (1999)

[2] Triplett, K.A., Ghiaasiaan, S.M., Abdel-Khalik, S.I., Sadowski, D.L., Gas-liquid two-phase flow in microchannels; Part II: void fraction and pressure drop. Int. J. Multiphase Flow, Vol. 25, pp. 395, (1999)

[3] Thulasidas, T.C., Abraham, M.A., Cerro, R.L., Bubble-train flow in capillaries of circular and square cross-section. Chem. Eng. Science, Vol. 50, No. 2, pp. 183, (1995)

[4] Thulasidas, T.C., Abraham, M.A., Cerro, R.L., Flow patterns in liquid slugs during bubble-train flow inside capillaries. Chem. Eng. Science, Vol. 52, No. 17, pp. 2947, (1997)

[5] Sabisch, W., Wörner, M., Grötzbach, G., Cacuci, D.G., 3D Volume-of-Fluid simulation of a wobbling bubble in a gas-liquid system of low Morton number. Fourth International Conference on Multiphase Flow, ICMF-2001, New Orleans, Louisiana, USA, June 2001

[6] Wörner, M., Sabisch, W., Grötzbach, G., Cacuci, D.G., Volume-averaged conservation equations for volume-of-fluid interface tracking. Fourth International Conference on Multiphase Flow, ICMF-2001, New Orleans, Louisiana, USA, June 2001